Journal of Materials Chemistry A

ROYAL SOCIETY OF CHEMISTRY

PAPER

View Article Online
View Journal

Cite this: DOI: 10.1039/d5ta09284a

Role of thermal gradient in interface stability of sodium metal electrodes

Aditya Singla, [a] Deep Chatterjee, [a] Bairav S. Vishnugopi,[a] Rachel E. Carter, [b] Corey T. Love[b] and Partha P. Mukherjee *[a]

The practical implementation of sodium (Na) metal electrodes is hindered by challenges such as dendrite growth and low coulombic efficiency. The morphological stability of the metal-electrolyte interface is strongly governed by coupled thermal phenomena that alter the underlying chemo-mechanical interactions. In this study, we investigate the role of operating temperature and thermal gradients in influencing ion transport, reaction kinetics, and interface stability during plating and stripping. While an increase in temperature improves ionic mobility and promotes creep-driven stabilization, it is demonstrated that higher temperatures also exacerbate reaction nonuniformity arising from heterogeneity in the solid electrolyte interphase (SEI). A comparative analysis between Na and lithium (Li) reveals that although Na exhibits higher creep rates, its larger molar volume leads to faster filament growth during deposition. Moreover, we show that localized heating within the SEI gives rise to thermal gradients near the metal-electrolyte interface, which in turn drive ionic flux *via* thermo-diffusion (Soret effect). It is found that thermo-diffusion can either suppress or amplify reaction heterogeneity depending on the direction and magnitude of thermal gradients. This work highlights the critical role of thermal design in enabling safe and stable operation of Na metal anodes across a wide range of operating conditions.

Received 14th November 2025
Accepted 21st June 2026

DOI: 10.1039/d5ta09284a

rsc.li/materials-a

1. Introduction

The increasing demand for energy storage technologies with low cost and high energy density has accelerated the development of alternative electrode materials and electrolyte systems for next-generation battery technologies.[1–3] As conventional lithium-ion batteries approach their theoretical limits, metal anode batteries have attracted significant attention due to their high specific capacity through the elimination of the porous anode matrix.[3–6] Conventionally, lithium (Li) has been used as the active material in such systems due to its low reduction potential (−3.04 V *versus* standard hydrogen electrode) and high theoretical specific capacity (~3860 mAh g^{-1}).[6–8] However, Li extraction poses environmental concerns and leads to increasing carbon footprints,[9,10] sparking interest in alternate active material chemistries.[11–13] In particular, sodium metal batteries (SMBs) are considered promising candidates because of the greater abundance and lower cost of sodium (Na) compared to Li.[14] Alongside these advantages, Na also offers a competitive specific capacity (~1165 mAh g^{-1}) and a low reduction potential (−2.7 V *versus* standard hydrogen electrode). Despite these advantages, the widespread adoption of SMBs remains hindered by critical challenges, primarily associated with dendritic growth due to interface instability, which undermines both performance and safety.[15–19]

The interface stability of Na metal anode is governed by the solid electrolyte interphase (SEI), which is formed during initial cycling.[20–24] The SEI serves as a barrier, regulating ion transport and preventing direct contact between the highly reactive Na metal and the electrolyte.[25–28] By serving as an ionically conducting, but electronically insulating layer, the presence of an SEI is essential in preventing unwanted side reactions that occur at the bare metal-electrolyte interface. For stable cycling, this layer must maintain mechanical integrity across repeated plating and stripping cycles.[29] However, heterogeneities in SEI composition and structure can lead to localized ionic flux, resulting in nonuniform Na deposition/dissolution and the growth of filaments/pits.[27,30–32] These localized features generate stress concentration that initiates SEI cracking, exposing fresh Na metal to the electrolyte and triggering further parasitic reactions.[33–35] This feedback loop alters SEI composition, amplifies reaction heterogeneity, and worsens interfacial instability. While SEI evolution and dendrite formation have been widely studied for Li metal systems, the intrinsic kinetic and thermodynamic coupling in Na systems remains less understood.[36–38]

Temperature plays a critical role in the performance of metal anode batteries, influencing ion transport, reaction kinetics,

[a]School of Mechanical Engineering, Purdue University, West Lafayette, IN 47907, USA. E-mail: pmukherjee@purdue.edu

[b]Chemistry Division, U.S. Naval Research Laboratory, Washington, D. C. 20375, USA

and the mechanical behavior of both the SEI and the electrode.[39–44] Elevated temperatures can reduce ionic resistance and enhance ionic mobility within the electrolyte, thereby promoting more uniform plating/stripping.[40,45] However, excessive temperatures can degrade the SEI, inducing morphological and compositional heterogeneities that increase overpotentials and promote irregular deposition.[45,47] Additionally, temperature-dependent chemo-mechanical interactions between the SEI and electrolyte further contribute to reaction nonuniformity. Such heterogeneities lead to dendrite formation, significantly compromising the safety and performance of metal batteries.[36,37] The mechanical response of the metal anode, including creep and plastic deformation, is also highly temperature-dependent and can strongly influence interface instability.[46] In this context, it may be mentioned that Li and Na exhibit different electrodeposition behaviors even under the same thermal conditions, which may be attributed to a difference in their physical properties.[48–51] Na exhibits a higher molar volume compared to Li (due to a larger atomic radius), which leads to a higher volume expansion for Na, as compared to Li for the same charge capacity. In addition, Na has a lower elastic modulus than Li and hence is a "softer" alkali metal. This leads to Na deposits being more prone to deformation, shape change, and stress relaxation than Li. Lastly, compared to Li, Na has a lower surface energy, which makes the formation of fresh interfaces thermodynamically more favorable. As a result, the reduced energetic penalty for surface creation in Na promotes interfacial roughening, leading to more heterogeneous deposition and nonuniform SEI formation.

Interestingly, performance degradation has also been observed at different temperatures in cases where SEI heterogeneity is minimal.[41] This suggests that other thermally driven mechanisms play a role in governing interface instability. One such factor is the presence of internal temperature gradients near the interface, arising from localized heat generation in the SEI. In addition to altering SEI formation and metal plating behavior,[52] these gradients can give rise to thermo-diffusion (Soret effect), which drives ionic flux in response to thermal gradients.[53–58] Thermodiffusion induced ionic flux is dependent on ionic concentration and on the magnitude of thermal gradients. Recent works on Na metal systems[57] has looked into the implications of linear temperature gradients on electrodeposition stability for Na metal electrodes; however previous studies have not taken into account the implications of an SEI layer. Additionally experimental work on the role of imposed external thermal gradients on Li-ion battery degradation[52] has been conducted, revealing a significant variation of battery performance with altering externally imposed temperature gradients. Thus, for the present work, accounting for a spatially varying SEI layer would lead to better characterization of deposition stability and would be more aligned with real systems, which is the purpose of the present study. Depending on the direction and magnitude of the gradient, thermo-diffusion can either stabilize the interface by homogenizing the current density or destabilize it by increasing the reaction heterogeneity. Notably, this effect can reverse between plating and stripping, such that the same thermal gradient induces opposite behavior in the two cases.

In this study, we investigate how thermal phenomena govern the complex interplay between temperature, SEI heterogeneity, and morphological stability. We employ a coupled electro-chemo-mechanical formulation to decipher the electrodeposition behavior for Na metal electrodes and employ instability metrics to characterize the deposition heterogeneity. Particular emphasis has been placed to elucidate the role of thermal gradients in modulating deposition instability. Both external operating conditions and internal temperature gradients play a critical role in influencing the electro-chemo-mechanical behavior of Na metal electrodes. We analyze the temperature-dependent modulation of SEI, interfacial heat dissipation, creep-driven stabilization (in both Na and Li), and the temporal dynamics of electrodeposition and dissolution. We show that electrochemical and thermal properties of the SEI, including ionic conductivity, thermal diffusivity, and interfacial thermal resistance, govern local heat generation, internal thermal gradients, and ionic flux pathways. The direction and magnitude of thermal gradients dictate the reaction heterogeneity and interface stability through thermo-diffusion or Soret effect. By systematically examining these chemo-mechanical and thermal interactions, we show the fundamental mechanisms underlying temperature-driven instability and identify design principles to enhance the performance and safety of Na metal electrodes.

2. Computational methods

The electro-chemo-mechanical model capturing the temperature-dependent transport through the electrolyte and SEI, reaction kinetics at the metal anode-electrolyte interface, mechanical stress in SEI and Na, and creep behavior of Na is given below.

The ionic transport in the electrolyte and the SEI is governed by electric potential, concentration, and thermal gradients. The conservation of charge in SEI and electrolyte gives:

$$\nabla\cdot(\kappa_i\nabla\phi_i) + \nabla\cdot(\kappa_{\mathrm{D},i}\nabla\ln c_i) + \nabla\cdot(\kappa_{T,i}\nabla T) = 0 \quad (1)$$

where κ_i and $\kappa_{\mathrm{D},i}$ are the effective ionic and diffusional conductivity, respectively, c_i is the ionic concentration, T is the temperature, and ϕ_i is the electric potential in the SEI or electrolyte ('i' denotes different components). The constant κ_T denotes the magnitude of ionic flux due to a given temperature gradient[53] and is defined as $\kappa_\mathrm{T} = \kappa S_\mathrm{ion}$, where S_ion is the effective Seebeck coefficient. Like solid conductors, where the Seebeck coefficient describes the voltage generated per unit temperature gradient due to electronic carriers, the measurable ionic Seebeck coefficient arises in electrolytes from Soret coefficients (thermo-diffusion parameters) of cations and anions.[58] The effective Seebeck coefficient is usually correlated to the Soret coefficient (defined next) and is taken as $S_\mathrm{ion} = S_T RT/F$, where S_T is the Soret coefficient.

The diffusion of Na^+ ions in the electrolyte and the SEI is given by species mass conservation (including the Soret effect):[55,57]

$$\frac{\partial c_i}{\partial t} + \nabla\cdot(D_i\nabla c_i) + \nabla\cdot(D_T c_i \nabla T) = 0 \quad (2)$$

Eqn (2) represents the transport of Na^+ in the presence of thermo-diffusion (Soret effect). Under an applied thermal gradient, the solvated Na^+ experiences an additional thermal gradient-induced flux due to this effect. Depending on the magnitude and sign of the Soret coefficient (which may vary with extrinsic factors such as solute composition and temperature), the solvated ions may behave in a thermophilic or a thermophobic manner. For instance, a positive value of the Soret coefficient would drive the solvated ions to move towards the low temperature zone in the domain, exhibiting thermophobic behavior. On the other hand, a negative Soret coefficient value implies that the solvated ions migrate to high temperature zones in the domain, that is, they exhibit thermophilic behavior. Using $S_T = \frac{D_T}{D}$, we can rewrite eqn (2) as:

$$\frac{\partial c_i}{\partial t} + \nabla\cdot(D_i(\nabla c_i + S_T c_i \nabla T) = 0 \quad (3)$$

where t is the time, and D_i is the effective diffusivity of the electrolyte or different components of SEI. In this study, the initial electrolyte concentration is uniform and therefore there is no contribution from concentration gradients in governing flux during the initial dynamics examined here. As a result, the interfacial response is governed predominantly by the thermally induced potential gradients rather than concentration gradients, which can play a major role over time.[57]

The electrochemical reaction at the Na-electrolyte interface follows the Butler–Volmer kinetics. The influence of mechanical stresses is incorporated through the mechanical overpotential, which alters the free-energy landscape.[59–61] Therefore, the reaction kinetics at the Na metal surface can be expressed using a modified form of the Butler–Volmer equation:

$$i_{rxn} = i_0\left\{\exp\left(\frac{F\eta_\phi}{2RT}\right)\exp\left(\frac{F\eta_\sigma}{RT}\right) - \exp\left(-\frac{F\eta_\phi}{2RT}\right)\right\} \quad (4)$$

where i_{rxn} is the reaction current density, i_0 is the exchange current density, η_ϕ is the electric overpotential, η_σ is the mechanical overpotential, F is the Faraday's constant, R is the universal gas constant, and T is the temperature. The electric and mechanical overpotentials at the anode interface are defined as:

$$\eta_\phi = \phi_s - \phi_e - U \quad (5)$$

$$\eta_\sigma = \frac{\Omega_{Na^+}\sigma_{h,e} - \Omega_{Na}\sigma_{h,Na}}{F} \quad (6)$$

where ϕ_s is the electric potential in the metal anode, ϕ_e is the electric potential in SEI, U is the equilibrium potential, Ω_{Na^+} and Ω_{Na} are the partial molar volumes of Na^+ in SEI and Na metal, respectively, $\sigma_{h,e}$ and $\sigma_{h,Na}$ are the hydrostatic stresses in the SEI and Na anode, respectively. For Li, the corresponding values of partial molar volumes and hydrostatic stresses are used in the same manner.

The stress fields within the SEI and Na are obtained by solving the mechanical equilibrium equations for a linear elastic, isotropic solid:

$$\nabla\cdot\boldsymbol{\sigma} = 0 \quad (7)$$

$$\boldsymbol{\sigma} = \frac{2\nu\mu}{1-2\nu}tr(\boldsymbol{\varepsilon})\boldsymbol{I} + 2\mu\boldsymbol{\varepsilon} \quad (8)$$

$$\boldsymbol{\varepsilon} = \frac{1}{2}\left[\nabla\boldsymbol{u} + (\nabla\boldsymbol{u})^T\right] \quad (9)$$

where $\boldsymbol{\sigma}$ is the stress tensor, $\boldsymbol{\varepsilon}$ is the strain tensor, μ is the shear modulus, ν is Poisson's ratio of SEI or Na, and $\boldsymbol{u}$ is the displacement vector. The linear elasticity formulation is appropriate at small length scales relevant to interface evolution in this study, where metals exhibit high hardness. The time-dependent stress response is separately captured through the creep formulation detailed below.

The creep deformation of Na is modeled using the following relation:[62–64]

$$\dot{\varepsilon} = \alpha C_r\left(\frac{p}{\beta}\right)^n \exp\left(\frac{-Q_c}{RT}\right) \quad (10)$$

where $\dot{\varepsilon}$ is the strain rate, C_r is a material constant, α and β are non-dimensional Bower factors, p is the stress in the material along creep direction, n is the stress exponent, and Q_c is the creep activation energy.

On simplifying:

$$\dot{\varepsilon} = A\left(\frac{p}{\sigma_0}\right)^n \quad (11)$$

where A is the effective creep constant for Na and σ_0 is the yield strength of Na.

The creep deformation is then given as:[33]

$$u_c = A\left(\frac{p}{\sigma_0}\right)^n \cdot u_{Na}\cdot t \quad (12)$$

where u_{Na} is the mechanical deformation of Na along the creep direction and Δt is the change in time.

The time-dependent growth of interface morphology due to Na plating/stripping and creep deformation is then evaluated as:

$$\frac{\partial h(x)}{\partial t} = \frac{-i_{rxn}(x)\Omega_{Na}}{zF} - \dot{u}_c(x) \quad (13)$$

where $h(x)$ is the height of newly plated/stripped Na, z is the number of valence electrons, and $\dot{u}_c(x)$ is the creep deformation rate of Na.

The induced thermal gradients due to heat generation in the SEI and electrolyte are obtained from the heat equation:

$$\rho C_p\frac{\partial T}{\partial t} = k\nabla^2 T + \dot{q} \quad (14)$$

where ρ is the density, C_p is the specific heat capacity, and k is the thermal conductivity of SEI or electrolyte. $\dot{q}$ denotes the ohmic heat generated within the domain and is given by $\dot{q} = i\cdot\nabla_\phi$, where i is the local current density.

It is to be noted that the present electro-chemo-mechanical model assumes a fixed SEI thickness distribution which is time invariant (Section S1). Thus, although the SEI layer is spatially inhomogeneous (with a sinusoidal distribution), it does not evolve in time. Further, we have assumed homogeneous thermal and transport SEI properties in the present study. This has been done in order to deconvolute the specific role of thermal gradients on electrodeposition stability of Na^+. Accounting for a spatial variation in SEI composition would lead to additional transport and thermal resistances, which make the specific role of temperature modulated electrodeposition stability harder to decouple. The coupled electro-chemo-mechanical equations (eqn (1)–(14)) have been solved using an open-source Finite Element framework (FEniCS) in python. Details of the boundary conditions and initial condition employed in the study, along with a schematic depiction of the same, have been included in Section S2 of the SI.

3. Results and discussion

Fig. 1 illustrates the coupled thermal, mechanical, and electrochemical processes that govern interface evolution during Na plating and stripping in the presence of an SEI layer at the metal-electrolyte interface. The formation of SEI happens in a spatially inhomogeneous manner leading to varying SEI thickness at different locations of the interface. While SEI is an ionically conductive layer, transport of Na^+ through the SEI is more sluggish than through the bulk electrolyte. During plating, low temperature conditions (Fig. 1a) lead to reduced ionic conductivity (through the bulk electrolyte and the SEI layer) and sluggish electrochemical kinetics, which limit transport and promote further heterogeneous Na deposition at the SEI-Na interface. As the temperature increases (Fig. 1b), ion mobility improves and the Na metal becomes more deformable, enabling creep-assisted stabilization. However, elevated temperatures also accelerate parasitic side reactions and SEI decomposition, leading to localized reaction hotspots and dendritic growth of Na. In the subsequent sections, we also explore the effects of thermal gradients on the electrodeposition behavior of Na, through thermo-diffusion (or the Soret effect) that directs ionic flux in the presence of thermal gradients. It is shown that during Na plating, a favorable gradient (∇T directed toward the interface and a positive Soret coefficient) drives ions away from high reaction regions, promoting more uniform interface growth (Fig. 1c). Conversely, an adverse gradient (∇T directed away from the interface) promotes a higher flux focusing and amplifies reaction heterogeneity and heat generation (Fig. 1d). During stripping, these effects are reversed, which has been discussed in detail ahead. We show that localized joule heating within the SEI (which is high relative to bulk electrolyte due to increased potential and concentration gradients in the SEI) can intrinsically lead to large spatial temperature gradients, leading to modulation of ionic transport. These scenarios highlight the complex interplay between thermal, electrochemical, and mechanical phenomena in dictating interface evolution. Optimizing thermal conditions is therefore essential to enhance the morphological stability of Na metal anodes.

Fig. 2 explores how temperature-SEI interactions dictate the extent of reaction heterogeneity at the Na/SEI interface. Ionic transport of Na^+ takes place through the bulk electrolyte and the SEI layer, however, transport is more sluggish through the SEI layer due to its low ionic diffusivity. The effect of temperature variation would thus modulate both the ionic transport through the SEI and the bulk electrolyte, the degree of modulation being dependent on their respective activation energies for ion transport. The activation energy ratio between SEI and electrolyte ($E_{t,\mathrm{SEI}}/E_{t,\mathrm{electrolyte}}$) thus alters the current distribution and interface morphology during Na plating. When the SEI has a higher temperature sensitivity ($E_{t,\mathrm{SEI}}/E_{t,\mathrm{electrolyte}} > 1$), increasing temperature leads to a higher rise in SEI conductivity (compared to the conductivity of electrolyte), thus mitigating the gap between the ionic diffusivity through the SEI and the bulk electrolyte, which leads to homogenization of ionic current distribution. This can be seen from the Arrhenius relation for electrochemical properties such as ionic conductivity, $k = k_0\exp(-E/RT)$, where a higher activation energy leads to a steeper increase in SEI conductivity for the same temperature rise (details in Section S1). As shown in Fig. 2a–c, this suppresses local current focusing and results in smoother, more homogeneous deposition. Fig. 2g shows the corresponding reaction current density at the interface for different temperatures, where heterogeneity diminishes with temperature. Additionally, the corresponding voltage drop across the electrolyte (Fig. S2) reduces with temperature, further indicating that increasing $k_{\mathrm{SEI}}/k_{\mathrm{electrolyte}}$ enhances uniformity.

Conversely, when the SEI has a lower activation energy than the electrolyte ($E_{t,\mathrm{SEI}}/E_{t,\mathrm{electrolyte}} < 1$), temperature rise enhances electrolyte conductivity more strongly, which further increases the pre-existing gap between the ionic diffusivity through the SEI and bulk electrolyte- promoting greater heterogeneity. The ratio $k_{\mathrm{SEI}}/k_{\mathrm{electrolyte}}$ decreases with temperature, leading to intensified flux localization through thinner SEI regions (Fig. 2d–f) and a higher reaction heterogeneity (Fig. 2h). It is noted that the voltage drop (Fig. S3) and the magnitude of current heterogeneity for this case are lower than in the previous case due to the inherently higher SEI conductivity resulting from its lower activation energy, since the fixed pre-exponential factor is calculated from a base value of temperature and activation energy ratio (Section S1). However, the relative enhancement in SEI transport with temperature is smaller, eventually amplifying instability at higher temperatures. It is noted that the thickness of the SEI is kept constant across all temperatures, and additional thermal degradation mechanisms at higher temperatures are not included since this analysis aims to understand the impact of temperature-dependent transport and kinetics on interface stability.

Fig. 2i and j shows the variation in interface stability (given by θ) across a range of activation energy (for transport) ratios and temperatures. Here, θ denotes the reaction heterogeneity and is defined as $\theta = i_{\max}/i_{\min}$, where $i_{\max}$ and $i_{\min}$ are the maximum and minimum reaction current density. Consequently, as θ approaches 1, it implies a relative homogenization

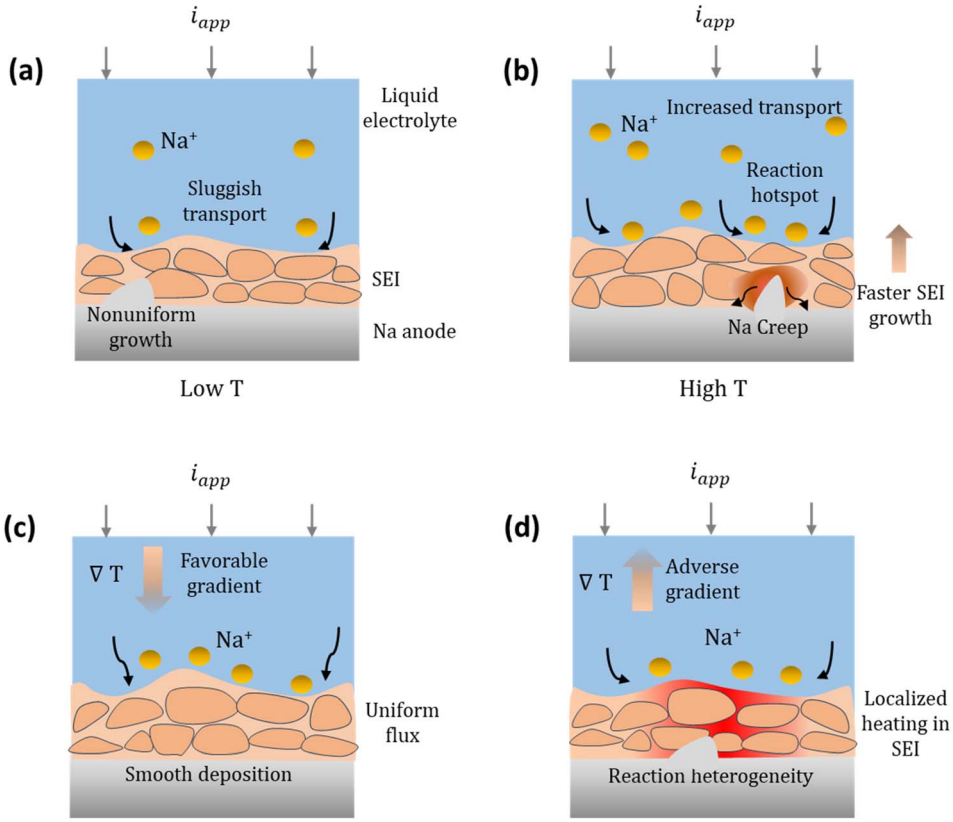

Fig. 1 Schematic illustrating the coupled thermal, electrochemical and mechanical effects during Na plating/stripping. Influence of (a) low and (b) high temperatures on ion transport, interface evolution, and Na creep. Impact of (c) favorable or (d) adverse thermal gradients on ionic flux redistribution due to the Soret effect during Na plating.

of the system. As shown in Fig. 2i, systems with higher $E_{t,\mathrm{SEI}}/E_{t,\mathrm{electrolyte}}$ transition toward more uniform deposition with increasing temperature as shown before. In contrast, Fig. 2j demonstrates that for a lower reaction activation energy (E_r), temperature accelerates interfacial reactions at thinner regions, resulting in localized hot spots and higher instability (θ values approaching 1.1 at low temperatures). These results suggest that for SEI, where reaction is more dominant, increasing temperature may destabilize the interface further. The parameters used in the model are listed in Table S1. Overall, these results emphasize that interface stability is not solely dictated by absolute conductivities, but rather by the relative thermally activated transport behavior of the SEI and the electrolyte. Carefully tailoring SEI chemistry and microstructure to optimize this interplay can enable more stable operation of Na metal anodes under varied thermal conditions.

In addition to electrochemical effects, mechanical response plays a critical role in governing interface stability. Fig. 3a shows the creep strain rate of Na and Li as a function of temperature, highlighting the pronounced thermo-mechanical sensitivity of Na due to its higher homologous temperature. At room temperature, the homologous temperature ($T_h = T/T_m$) for Na is approximately 0.8, compared to ~0.66 for Li, indicating that Na functions closer to its melting point. This inherently makes Na more susceptible to diffusional creep with a faster self-diffusion and higher deformation rate, whereas Li predominantly undergoes dislocation-based creep.[62] A higher T_h for Na also implies that the activation energy for creep is close to the activation energy for lattice diffusion (~44 kJ mol^{-1}). On the other hand, for Li, creep is governed by dislocation core diffusion, leading to lower values of creep activation energy barrier (~33 kJ mol^{-1}) compared to activation energy for lattice diffusion in Li. As a result, Na exhibits higher time-dependent creep deformation than Li, especially at elevated temperatures (due to higher diffusional creep and larger activation energy values for Na). This thermal activation of creep can mitigate morphological instability by redistributing material from high-stress regions (protrusions) to low-stress regions (valleys), serving as a stabilizing mechanism. However, Na also has a higher molar volume than Li, leading to greater volume expansion during deposition and faster interface growth, which can counteract some of the stabilizing effects of creep, as shown ahead.

Fig. 3b–i and S4–S7 compare the dynamic interface evolution and mechanical response of Li and Na at two different temperatures (0 °C and 60 °C). Fig. 3b–e shows the interface evolution of Li and Na electrodes at 0 °C and 60 °C. Li exhibits more nonuniform interface morphology at lower temperatures but undergoes interface smoothing at 60 °C as thermally activated creep becomes more significant. In contrast, although Na exhibits active creep even at lower temperatures due to its high

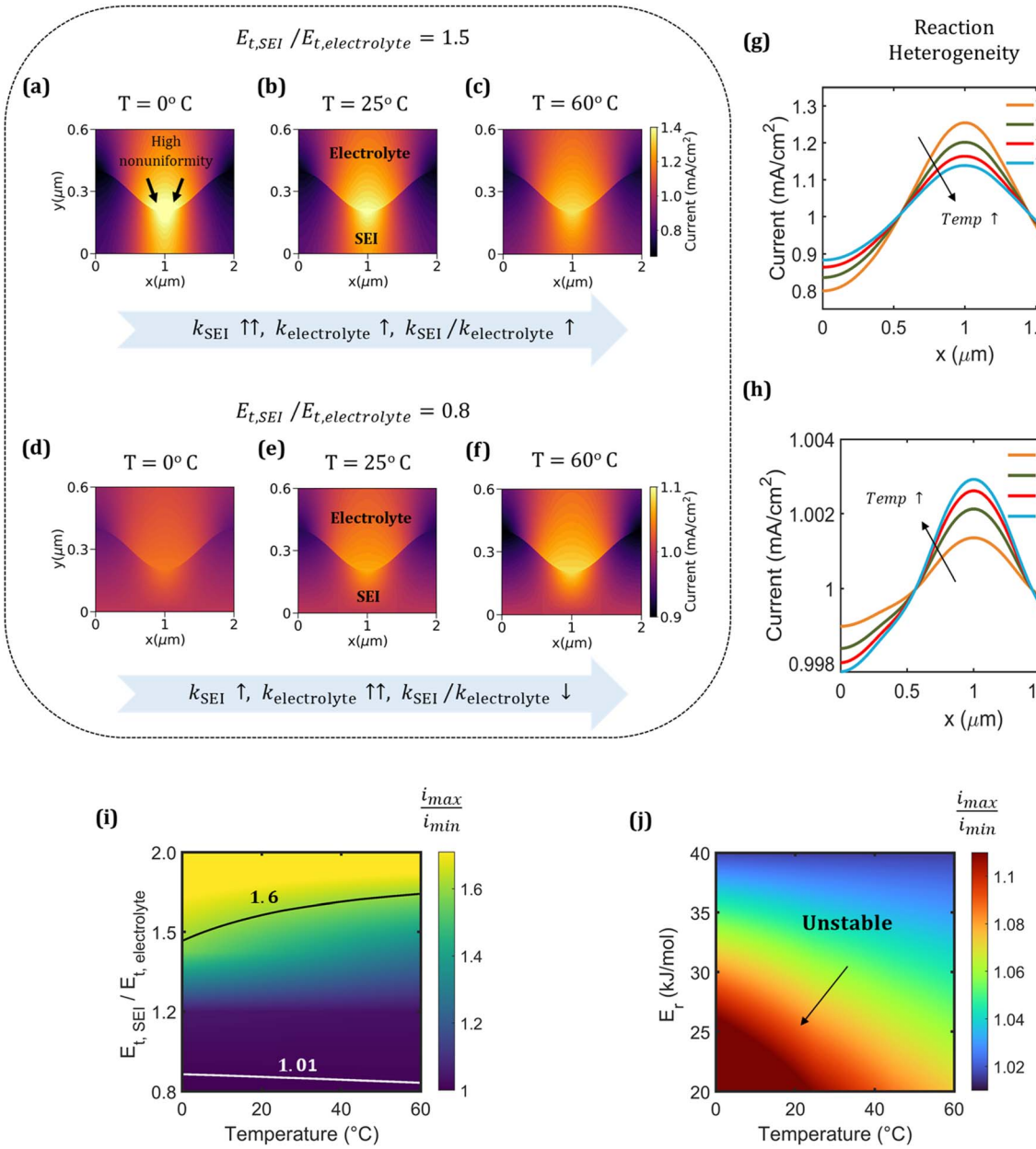

Fig. 2 Effect of temperature-dependent SEI interactions on interface stability. Current distribution in the SEI during Na plating for activation energy ratio, $E_{t,SEI}/E_{t,electrolyte} > 1$ at (a) $T = 0$ °C, (b) $T = 25$ °C and (c) $T = 60$ °C. Current distribution in the SEI during Na plating for activation energy ratio, $E_{t,SEI}/E_{t,electrolyte} < 1$ at (d) $T = 0$ °C, (e) $T = 25$ °C and (f) $T = 60$ °C. (g and h) Corresponding reaction current density at the Na-SEI interface for different temperatures for the two cases. (i and j) Contour plots showing the effect of temperature, activation energy for transport, and activation energy for reaction on interface stability, denoted by $\theta = i_{max}/i_{min}$. Table S1 lists the parameters used in this study.

homologous temperature, the larger molar volume of Na plays a more dominant role, resulting in faster interface growth compared to Li. Therefore, while Li transitions from unstable to smoother morphologies with increasing temperature, Na shows relatively less variation in interface amplitude between 0 °C and 60 °C.

Fig. 3f–i shows the corresponding hydrostatic stress distributions in the SEI during Na and Li electrodeposition. At lower temperatures, stress localization is higher near protrusions, which can promote reaction heterogeneity and mechanical failure of the SEI. At elevated temperatures, thermally activated creep in Li leads to more diffuse stress fields and lesser stresses (Fig. 3g). However, for Na (Fig. 3i), hydrostatic stresses remain relatively high even at 60 °C, driven by accelerated interface growth due to its larger molar volume, despite higher creep deformation. Fig. 3j and k shows the temporal evolution of filament height (Δh) and maximum hydrostatic stress for both metals. Na exhibits faster morphological growth and higher peak stress at both temperatures. In contrast, Li demonstrates delayed stress buildup and smoother morphological evolution

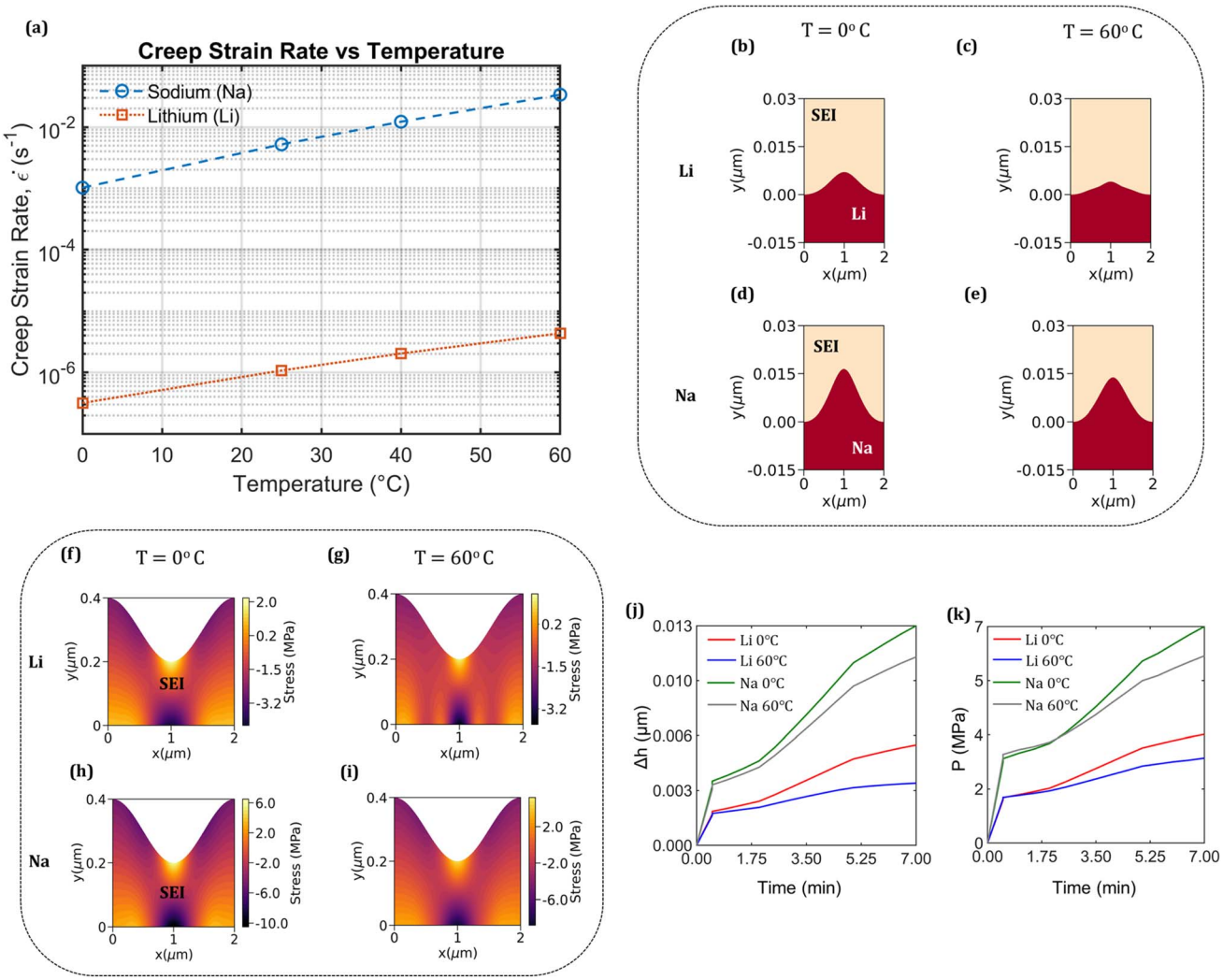

Fig. 3 Temperature-dependent interface evolution in Na and Li metal anodes. (a) Creep strain rate of Na and Li as a function of temperature. Interface morphology at $t = 7$ minutes for $T = 0$ °C and $T = 60$ °C for (b and c) Li and (d and e) Na. Hydrostatic stress distribution in the SEI at $t = 7$ minutes for $T = 0$ °C and $T = 60$ °C for (f, g) Li and (h and i) Na. Evolution of (j) filament height (Δh) and (k) maximum hydrostatic stress for Na and Li at $T = 0$ °C and $T = 60$ °C.

at elevated temperatures, implying the onset of creep and its stabilizing effect over time. These results underscore the critical role of temperature in shaping not only transport and kinetics, but also the mechanical landscape at the interface, thereby modulating stability pathways in SMBs.

In this study, we assume a chemically uniform SEI with the same electrochemical and mechanical properties for both Li and Na to isolate the effect of electrode material properties (*e.g.*, molar volume, creep behavior) on interface evolution. While the SEI is highly dependent on the choice of electrolyte and can vary significantly in composition and structure for both metals, experimental studies suggest that Na typically forms a more chemically heterogeneous SEI than Li, potentially due to its higher reactivity.[22,26] We do not consider the chemical heterogeneity of SEI in our model, which will likely lead to even more unstable growth in Na.[30] In addition, in the analysis presented in Fig. 3, we do not vary any reaction parameters with temperature and take $E_{t,\mathrm{SEI}}/E_{t,\mathrm{electrolyte}} = 1$ (so that the conductivity ratio of SEI and electrolyte remains the same) in order to isolate and highlight the role of mechanics.

So far, we've analyzed the effect of thermal modulation on deposition stability, through ionic transport, reaction rate, and creep variation for different alkali metals. Now, we'll be specifically looking at how imposed thermal gradients might affect the deposition dynamics due to the Soret effect. Imposed thermal gradients across the SEI would give rise to a thermo-diffusive flux (i_T) that alters ionic current distribution during electrodeposition and dissolution (schematic representation in Fig. 1c and d). Fig. 4a–c shows applied temperature gradients ($\nabla T = 10^4$ K m^{-1}, 0, -10^4 K m^{-1}) across the electrolyte with a positive Soret coefficient at a base temperature of 25 °C and $E_{t,\mathrm{SEI}}/E_{t,\mathrm{electrolyte}} = 1.5$, which corresponds to the range of thermal gradients reported in previous studies.[52,65,66] The direction of i_T reverses depending on the sign of ∇T. During

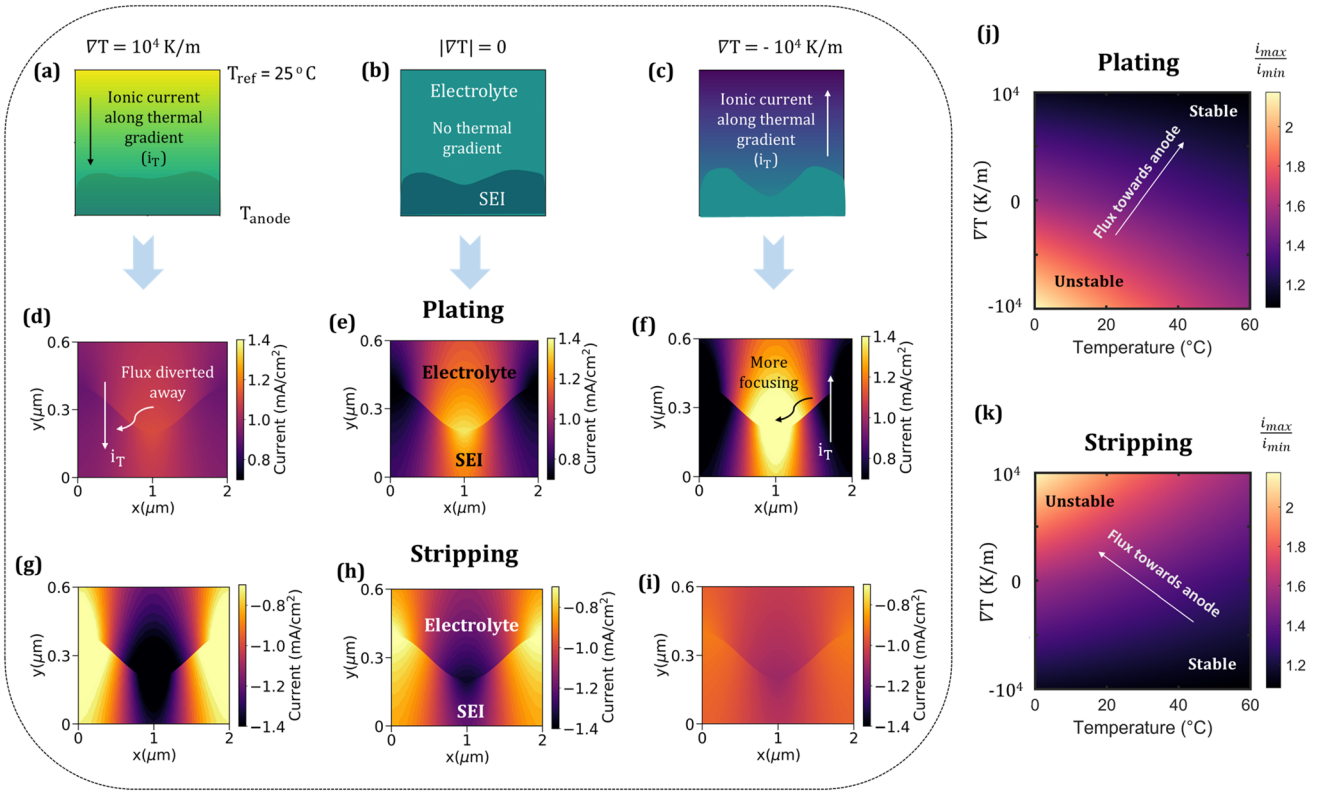

Fig. 4 Influence of applied thermal gradients on thermo-diffusion-driven interface evolution. Applied temperature gradient profiles for ∇T = (a) 10^4 K m^{-1}, (b) 0, and (c) -10^4 K m^{-1} across the domain. Corresponding current distribution during Na (d–f) plating and (g–i) stripping for each gradient direction. Combined influence of ∇T and base temperature on interface stability, $\theta = i_{max}/i_{min}$ for (j) plating and (k) stripping.

plating, a constant thermal flux due to thermal gradient directed toward the anode ($\nabla T > 0$) drives ions away from thinner SEI regions, redistributing flux and suppressing localized deposition (Fig. 4d), while a gradient directed away from the anode ($\nabla T < 0$) further focuses flux and enhances growth instability (Fig. 4f). In the absence of any thermal gradient (Fig. 4e), deposition/dissolution is primarily governed by electric field-driven transport arising from SEI heterogeneity. It is to be noted that the study has been carried out under galvanostatic conditions, which implies that as i_T varies, the net ionic flux redistribution still has to lead to a constant plating/stripping current across the interface. Thus when i_T (which is spatially uniform) is directed towards the SEI during plating, the current focusing occurring through the thinnest region of the SEI is alleviated, while when i_T acts in the opposite direction, ionic current due to potential and concentration gradients increase in order to still lead to the same plating current, leading to exacerbated ionic focusing of ionic current through the thinnest SEI region, where it encounters the least resistance. This phenomenon of Soret effect-induced stabilization has been observed in prior experimental studies where an adverse thermal gradient with a cold anode and a warm cathode led to faster cell degradation.[52] Recent computational studies[57,58] on Na and Li ion batteries also substantiate this behavior, although they do not consider the unique effect of the SEI. During stripping (Fig. 4g–i), the impact of thermo-diffusion is reversed: thermal gradient directed toward the anode ($\nabla T > 0$) increases nonuniformity, whereas opposite gradients direct more ionic flux from valleys, aiding in homogenizing the dissolution front.

Fig. 4j and k quantifies the degree of reaction localization ($\theta = i_{max}/i_{min}$) as a function of ∇T and base temperature, illustrating that thermo-diffusion becomes less effective at higher temperatures. The electrochemical properties inherently improve with temperature and begin to stabilize the interface, thereby reducing the relative impact of applied thermal gradients. Therefore, the overall stabilization is dictated by the ratio $\nabla T/T$. For plating (Fig. 4j), positive gradients stabilize the interface, whereas for stripping (Fig. 4k), stability improves under negative gradients directed away from the anode.

In practice, thermal gradients can develop intrinsically owing to the poor ion transport through the SEI and low thermal conductivity. Low ionic diffusivity (and ionic conductivity) leads to increased concentration and potential gradients in the SEI region, which then increases the ohmic heat generation. The heat generation within the SEI can induce thermal gradients near the interface; while Na metal dissipates heat quickly due to its high thermal conductivity, the bulk electrolyte being less thermally conductive leads to a temperature variation across the SEI layer. This mismatch of thermal conductivity on either side of the SEI, coupled with a poor thermal conductivity of the SEI layer itself leads to the generation of large thermal gradients. In particular, poor thermal conductivity within the

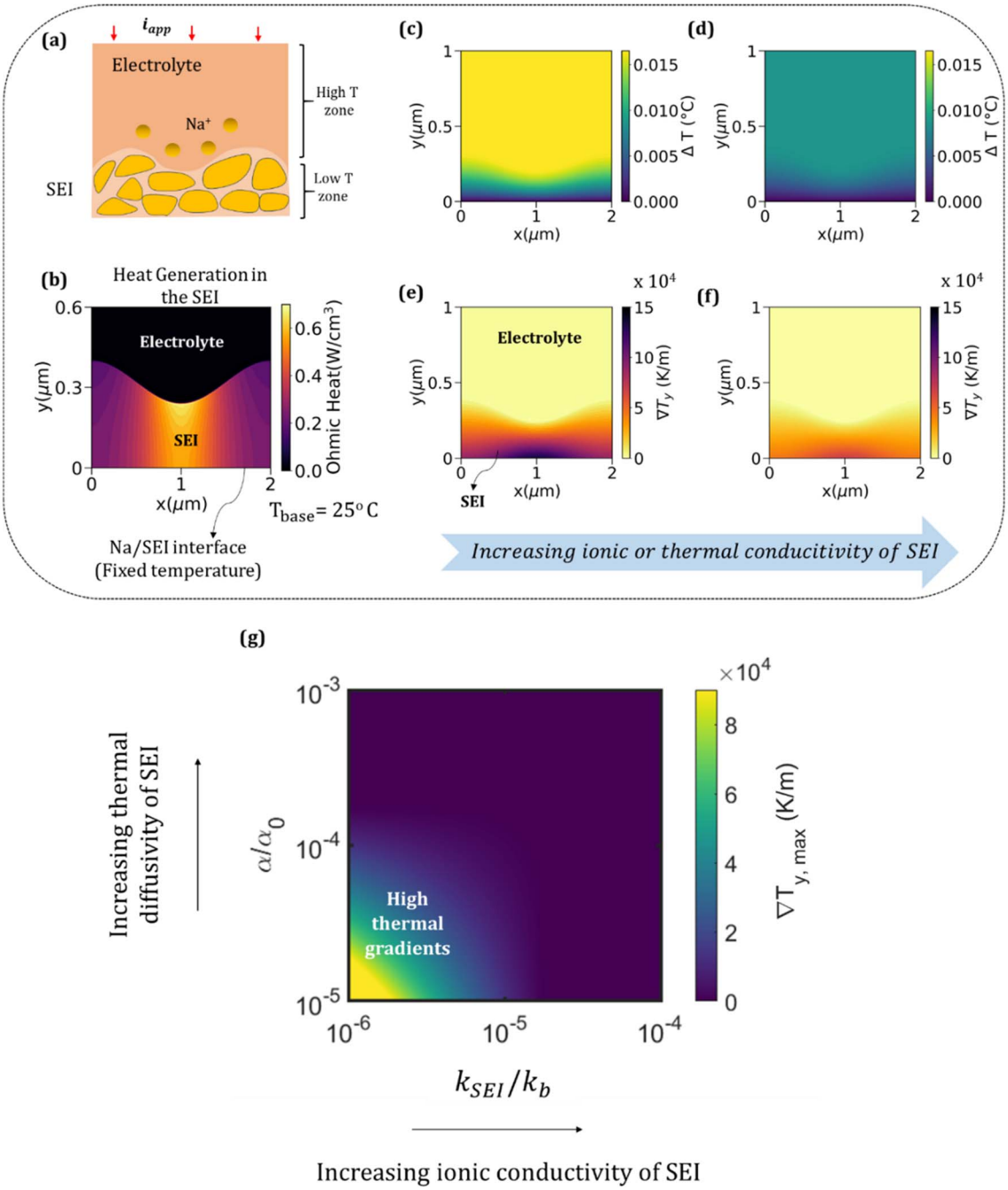

Fig. 5 (a) Schematic representation of temperature rise due to internal heat generation in the SEI and electrolyte. (b) Ohmic heat generation in the SEI at 25 °C base temperature. (c and d) Resulting temperature distributions across the SEI-electrolyte domain for SEI with lower and higher thermal and ionic conductivity, respectively. (e and f) Corresponding vertical thermal gradient profiles (∇T_y) showing sharper gradients in high-resistance SEI and reduced gradients in low-resistance SEI. (g) Maximum vertical thermal gradient ($\nabla T_{y,max}$) as a function of SEI ionic conductivity and thermal diffusivity.

SEI can limit heat flow toward the metal, while dissipation into the bulk electrolyte can elevate the electrolyte temperature relative to the SEI, creating a thermal gradient directed toward the interface (Fig. 5a). The ohmic heat generation in the SEI under a uniform applied current at 25 °C base temperature is shown in Fig. 5b. The highest localized heating occurs near the protrusion tip due to the intensified potential gradient in regions with reduced thickness, where ion conduction becomes more concentrated. The Na-SEI interface is maintained at a constant temperature owing to the high thermal conductivity of Na metal, which acts as an effective heat sink. As a result, the thermal gradients primarily develop along the SEI thickness direction (y-axis), forming a vertical profile from the interface toward or away from the bulk electrolyte. Fig. 5c and d shows the resulting temperature distribution (with respect to the base temperature) within the electrolyte-SEI domain for two different

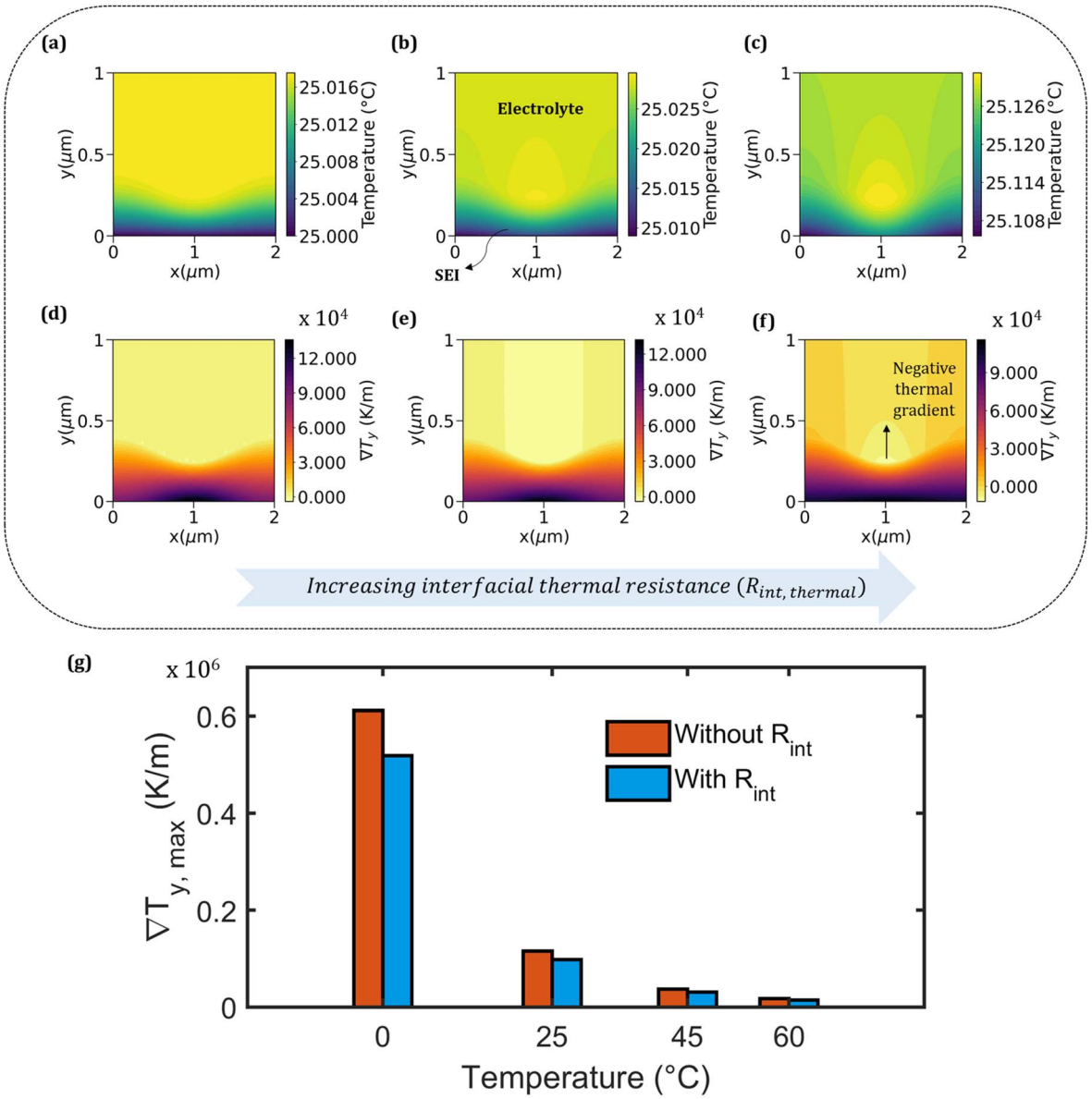

Fig. 6 (a–c) Temperature distribution across the SEI-electrolyte domain with increasing interfacial thermal resistance, R_{int}. (d–f) Corresponding vertical thermal gradients (∇T_i). (g) Maximum vertical thermal gradient ($\nabla T_{y,max}$) at different temperatures, comparing systems with and without R_{int}.

scenarios: (i) SEI with lower ionic/thermal conductivity, and (ii) SEI with higher ionic/thermal conductivity. The ionic conductivity of SEI, $k_{SEI}/k_b = 10^{-5}$ and 2×10^{-5} for Fig. 5c–f, respectively ($k_b = 0.005$ mS cm^{-1} denotes a base value of SEI ionic conductivity); similar trends are obtained on varying the thermal conductivity. Although heat is dissipated into the surrounding domains, the poor thermal transport of the SEI (due to low thermal conductivity) or high heat generation (due to low ionic conductivity) causes local temperature elevation near the hotspot. Fig. 5e and f illustrates the corresponding vertical temperature gradient profiles, ∇T_y, within the system. A lower SEI conductivity produces a steep temperature gradient near the peak of the SEI (Fig. 5e), which drives thermo-diffusive transport that can significantly affect local reaction distribution. In contrast, when the SEI has improved thermal or ionic conductivity (Fig. 5f), the temperature distribution is more uniform and gradients are suppressed. Fig. 5g shows the maximum vertical thermal gradient ($\nabla T_{y,max}$) as a function of SEI ionic conductivity and thermal diffusivity ($\alpha = k_{thermal}/\rho C_p$), normalized by k_b and α_0, respectively. Here, $k_{thermal}$ is the ionic conductivity of the SEI, ρ is the density, C_p is the specific heat capacity, and α_0 is the thermal conductivity of Na. Poorly conductive SEIs, both thermally and ionically, are highly susceptible to forming sharp thermal gradients. This analysis highlights the importance of optimizing SEI properties to mitigate local thermal inhomogeneities that could otherwise amplify nonuniform current and induce instability during cycling.

Fig. 6 illustrates the impact of interfacial thermal resistance (R_{int}) at the Na-SEI-electrolyte on the development of thermal gradients. While Fig. 5 assumed ideal contact with no resistance at the interfaces, real systems often possess finite thermal resistance that hinders heat flux continuity, especially at poorly bonded or nonconformal interfaces. The nanoscale SEI can also introduce substantial resistance at the interface. Fig. 6a–c shows the steady-state temperature distribution across the electrolyte and SEI for increasing values of $R_{int} = 0$ (no resistance), 10^{-5}, and 10^{-4} Km^2 W^{-1} (for ionic conductivity of SEI, $k_{SEI}/k_b = 2 \times 10^{-5}$). As R_{int} increases, heat dissipation into the metal is impeded, causing a localized temperature rise at the SEI-electrolyte interface. Fig. 6d–f shows the corresponding vertical thermal gradients, ∇T_y. Notably, for high R_{int} (Fig. 6f), the direction of the thermal gradient across the SEI reverses, resulting in a negative ∇T (away from the anode). This reversal can fundamentally alter the direction of thermo-diffusion and the resulting interface stability (Fig. 4). Although the absolute temperature rise remains small, the nanoscale SEI thickness leads to large local gradients, which are sufficient to promote significant Soret-driven transport.

Fig. 6g compares the peak vertical gradient ($\nabla T_{y,max}$) across different base temperatures for systems with R_{int} ($=10^{-5}$ Km^2 W^{-1}) and without R_{int}. At lower temperatures, the effect of R_{int} is more pronounced, producing steeper gradients. At elevated temperatures, however, improved properties reduce these gradients, thereby diminishing the impact of thermo-diffusion. These results highlight that, beyond bulk SEI properties, the interfacial contact plays a critical role in governing thermal-driven effects in SMBs.

4. Conclusion

This work presents a comprehensive chemo-mechano-thermal framework to elucidate the role of temperature and thermal gradients in Na metal electrodes. While elevated temperatures enhance transport, reaction kinetics, and creep deformation, the overall morphological stability is strongly dictated by the temperature-dependent mechanical and electrochemical response of the SEI, electrolyte and metal anode. A more thermally responsive SEI that exhibits a larger conductivity increase with temperature relative to the electrolyte stabilizes the interface, whereas a less sensitive SEI increases reaction heterogeneity and promotes unstable growth. Even though compositional variability in the SEI domain has not been considered in the present study, the general results are largely expected to show a similar trend even when a chemically non-uniform SEI composition is considered, which may lead to thermal and ionic transport modulation in the SEI layer. While temperature-dependent creep deformation contributes to interface stabilization, the intrinsic properties of the metal electrode, such as molar volume and homologous temperature, also play a critical role in governing growth dynamics. Compared to Na, Li has a lower molar volume, resulting in more stable morphological evolution despite having a lower creep-driven stabilization. Additionally, applied or induced thermal gradients (due to localized heat generation in the SEI) introduce thermo-diffusion effects, which can either suppress or amplify morphological nonuniformities depending on the directionality of thermal gradients during Na plating and stripping. For plating, thermal gradients directing ions towards the anode lead to stabilization and *vice versa*. For stripping, the scenario is reversed such that thermodiffusion which acts to drive ions away from the anode enhance the stripping stability. While direct experimental evidence of the effect of thermal gradients on the modulation of electrodeposition behavior in metal electrodes is presently absent, it is possible to conduct such an experiment and compare changes in deposition dynamics with varying imposed thermal gradients. However, care must be taken to deconvolute the effect of imposed thermal gradients from the effect of temperature induced thermal and transport property modulation to selectively understand the role of thermal gradients. The interfacial thermal resistance at the Na-SEI interface further influences these gradients by altering local heat dissipation. Together, these findings highlight the importance of thermal phenomena in governing interface stability and morphological evolution under varied operating conditions in Na metal electrodes.

Conflicts of interest

The authors declare no conflict of interest.

Data availability

The data supporting this article have been included as part of the supplementary information (SI). Supplementary information: Section S1 – properties of SEI, electrolyte, Na, and Li; Table S1 – list of parameters and properties used in the model; Section S2 – boundary conditions and initial conditions. Section S3 – supporting results. See DOI: https://doi.org/10.1039/d5ta09284a.

Acknowledgements

Financial support in part from the Office of Naval Research (ONR), grant: N00014-23-1-2608, is gratefully acknowledged. P. P. M. would like to thank Dr. Michele Anderson from ONR for the support.

References

1 K. Amine, R. Kanno and Y. H. Tzeng, Rechargeable lithium batteries and beyond: progress, Challenges, and future directions, *MRS Bull.*, 2014, **39**, 395–405.
2 S. Chu and A. Majumdar, Opportunities and challenges for a sustainable energy future, *Nature*, 2012, **488**, 294–303.
3 N. S. Choi, *et al.*, Challenges facing lithium batteries and electrical double-layer capacitors, *Angew Chem., Int. Ed. Engl.*, 2012, **51**, 9994–10024.
4 F. Degen, M. Winter, D. Bendig and J. Tübke, Energy consumption of current and future production of lithium-ion and post lithium-ion battery cells, *Nat. Energy*, 2023, **8**, 1284–1295.

5 M. N. He, *et al.*, Industry needs for practical lithium-metal battery designs in electric vehicles, *Nat. Energy*, 2024, **9**, 1199–1205.
6 W. Xu, *et al.*, Lithium metal anodes for rechargeable batteries, *Energy Environ. Sci.*, 2014, **7**, 513–537.
7 M. Wang, F. Zhang, C. S. Lee and Y. Tang, Low-Cost Metallic Anode Materials for High Performance Rechargeable Batteries, *Adv. Energy Mater.*, 2017, **7**, 1700536.
8 Y. Tian, *et al.*, Recently advances and perspectives of anode-free rechargeable batteries, *Nano Energy*, 2020, **78**, 105344.
9 Y. Guo, H. Li and T. Zhai, Reviving Lithium-Metal Anodes for Next-Generation High-Energy Batteries, *Adv. Mater.*, 2017, **29**, 1700007.
10 X. B. Cheng, R. Zhang, C. Z. Zhao and Q. Zhang, Toward Safe Lithium Metal Anode in Rechargeable Batteries: A Review, *Chem. Rev.*, 2017, **117**, 10403–10473.
11 X. Zhang, Y. Yang and Z. Zhou, Towards practical lithium-metal anodes, *Chem. Soc. Rev.*, 2020, **49**, 3040–3071.
12 L. Peiseler, *et al.*, Carbon footprint distributions of lithium-ion batteries and their materials, *Nat. Commun.*, 2024, **15**, 10301.
13 M. L. Vera, W. R. Torres, C. I. Galli, A. Chagnes and V. Flexer, Environmental impact of direct lithium extraction from brines, *Nat. Rev. Earth Environ.*, 2023, **4**, 149–165.
14 A. Patrike, P. Yadav, V. Shelke and M. Shelke, Research Progress and Perspective on Lithium/Sodium Metal Anodes for Next-Generation Rechargeable Batteries, *ChemSusChem*, 2022, **15**, e202200504.
15 A. Yao, S. M. Benson and W. C. Chueh, Critically assessing sodium-ion technology roadmaps and scenarios for techno-economic competitiveness against lithium-ion batteries, *Nat. Energy*, 2025, **10**, 404–416.
16 T. Yang, D. Luo, Y. Liu, A. Yu and Z. Chen, Anode-free sodium metal batteries as rising stars for lithium-ion alternatives, *iScience*, 2023, **26**, 105982.
17 H. Y. Kang, *et al.*, Update on anode materials for Na-ion batteries, *J. Mater. Chem. A*, 2015, **3**, 17899–17913.
18 S. J. Lee, *et al.*, Stable sodium-metal batteries with a hierarchical structured electrode toward reversible confinement of Na dendrites, *Energy Storage Mater.*, 2024, **65**, 103047.
19 M. Ali, *et al.*, Recent development in sodium metal batteries: challenges, progress, and perspective, *Mater. Today*, 2025, **88**, 730–751.
20 C. Y. Bao, *et al.*, Solid Electrolyte Interphases on Sodium Metal Anodes, *Adv. Funct. Mater.*, 2020, **30**, 2004891.
21 Q. Cheng, *et al.*, Criticality of solid electrolyte interphase in achieving high performance of sodium-ion batteries, *Chem. Eng. J.*, 2023, **457**, 141097.
22 E. Matios, H. Wang, C. L. Wang and W. Y. Li, Enabling Safe Sodium Metal Batteries by Solid Electrolyte Interphase Engineering: A Review, *Ind. Eng. Chem. Res.*, 2019, **58**, 9758–9780.
23 E. Peled and S. Menkin, Review-SEI: Past, Present and Future, *J. Electrochem. Soc.*, 2017, **164**, A1703–A1719.
24 S. Choudhury, *et al.*, Designing solid-liquid interphases for sodium batteries, *Nat. Commun.*, 2017, **8**, 898.
25 B. Lee, E. Paek, D. Mitlin and S. W. Lee, Sodium Metal Anodes: emerging Solutions to Dendrite Growth, *Chem. Rev.*, 2019, **119**, 5416–5460.
26 W. Liu, P. C. Liu and D. Mitlin, Review of Emerging Concepts in SEI Analysis and Artificial SEI Membranes for Lithium, Sodium, and Potassium Metal Battery Anodes, *Adv. Energy Mater.*, 2020, **10**, 2002297.
27 M. J. Hou, *et al.*, Research progress of solid electrolyte interphase for sodium metal anodes, *Chem. Eng. J.*, 2023, **475**, 146227.
28 B. Yadav, C. B. Soni, S. Bera, H. Kumar and V. Kumar, Direct observation of sodium dendrites to decipher the complicated behavior of electrolyte systems, *Electrochim. Acta*, 2024, **507**, 145212.
29 C. Bommier and X. Ji, Electrolytes, SEI Formation, and Binders: a Review of Nonelectrode Factors for Sodium-Ion Battery Anodes, *Small*, 2018, **14**, e1703576.
30 A. Singla, K. G. Naik, B. S. Vishnugopi and P. P. Mukherjee, Heterogeneous Solid Electrolyte Interphase Interactions Dictate Interface Instability in Sodium Metal Electrodes, *Adv. Sci.*, 2024, **11**, e2404887.
31 L. Y. Kuo, A. Moradabadi, H. F. Huang, B. J. Hwang and P. Kaghazchi, Structure and ionic conductivity of the solid electrolyte interphase layer on tin anodes in Na-ion batteries, *J. Power Sources*, 2017, **341**, 107–113.
32 J. Lee, J. Kim, S. Kim, C. Jo and J. Lee, A review on recent approaches for designing the SEI layer on sodium metal anodes, *Mater. Adv.*, 2020, **1**, 3143–3166.
33 A. Singla, K. G. Naik, B. S. Vishnugopi and P. P. Mukherjee, Chemo-Mechanics Interplay Dictates Interface Instability and Asymmetry in Plating and Stripping of Sodium Metal Electrodes, *Adv. Funct. Mater.*, 2025, **35**, 2418033.
34 X. Shen, *et al.*, The Failure of Solid Electrolyte Interphase on Li Metal Anode: structural Uniformity or Mechanical Strength?, *Adv. Energy Mater.*, 2020, **10**, 1903645.
35 Y. Y. Liu, *et al.*, Electro-Chemo-Mechanical Modeling of Artificial Solid Electrolyte Interphase to Enable Uniform Electrodeposition of Lithium Metal Anodes, *Adv. Energy Mater.*, 2022, **12**, 2103589.
36 J. F. Ding, *et al.*, A review on the failure and regulation of solid electrolyte interphase in lithium batteries, *J. Energy Chem.*, 2021, **59**, 306–319.
37 B. Horstmann, *et al.*, Strategies towards enabling lithium metal in batteries: interphases and electrodes, *Energy Environ. Sci.*, 2021, **14**, 5289–5314.
38 S. J. An, *et al.*, The state of understanding of the lithium-ion-battery graphite solid electrolyte interphase (SEI) and its relationship to formation cycling, *Carbon*, 2016, **105**, 52–76.
39 G. Li, X. Lou, C. Peng, C. Liu and W. Chen, Interface chemistry for sodium metal anodes/batteries: a review, *Chem. Synth.*, 2022, **2**, 16.
40 Z. J. Hong and V. Viswanathan, Prospect of Thermal Shock Induced Healing of Lithium Dendrite, *ACS Energy Lett.*, 2019, **4**, 1012.
41 L. Li, *et al.*, Self-heating-induced healing of lithium dendrites, *Science*, 2018, **359**, 1513–1516.

42 P. Li *et al.*, *Synergistic Effects of Salt Concentration and Working Temperature towards Dendrite-free Lithium Deposition*, Research (Wash D C), 2019, 7481319.
43 J. B. Hou, M. Yang, D. Y. Wang and J. L. Zhang, Fundamentals and Challenges of Lithium Ion Batteries at Temperatures between-40 and 60 °C, *Adv. Energy Mater.*, 2020, **10**.
44 K. Yan, *et al.*, Temperature-Dependent Nucleation and Growth of Dendrite-Free Lithium Metal Anodes, *Angew Chem. Int. Ed. Engl.*, 2019, **58**, 11364–11368.
45 B. S. Vishnugopi, F. Hao, A. Verma and P. P. Mukherjee, Double-Edged Effect of Temperature on Lithium Dendrites, *ACS Appl. Mater. Interfaces*, 2020, **12**, 23931–23938.
46 A. Masias, N. Felten, R. Garcia-Mendez, J. Wolfenstine and J. Sakamoto, Elastic, plastic, and creep mechanical properties of lithium metal, *J. Mater. Sci.*, 2018, **54**, 2585–2600.
47 M. T. F. Rodrigues, *et al.*, A materials perspective on Li-ion batteries at extreme temperatures, *Nat. Energy*, 2017, **2**.
48 L. B. Ma, *et al.*, Dendrite-free lithium metal and sodium metal batteries, *Energy Storage Mater.*, 2020, **27**, 522–554.
49 M. Jackle and A. Gross, Microscopic properties of lithium, sodium, and magnesium battery anode materials related to possible dendrite growth, *J. Chem. Phys.*, 2014, **141**, 174710.
50 L. Vitos, A. V. Ruban, H. L. Skriver and J. Kollár, The surface energy of metals, *Surf. Sci.*, 1998, **411**, 186–202.
51 D. Gaissmaier, M. van den Borg, D. Fantauzzi and T. Jacob, Microscopic Properties of Na and Li-A First Principle Study of Metal Battery Anode Materials, *ChemSusChem*, 2020, **13**, 771–783.
52 R. Carter, *et al.*, Directionality of thermal gradients in lithium-ion batteries dictates diverging degradation modes, *Cell Rep. Phys. Sci.*, 2021, **2**.
53 J. Newman, Thermoelectric Effects in Electrochemical Systems, *Ind. Eng. Chem. Res.*, 1995, **34**, 3208–3216.
54 M. A. Rahman and M. Z. Saghir, Thermodiffusion or Soret effect: Historical review, *Int. J. Heat Mass Transfer*, 2014, **73**, 693–705.
55 L. Rezende Franco, A. L. Sehnem, A. M. Figueiredo Neto and K. Coutinho, Molecular Dynamics Approach to Calculate the Thermodiffusion (Soret and Seebeck) Coefficients of Salts in Aqueous Solutions, *J. Chem. Theory Comput.*, 2021, **17**, 3539–3553.
56 S. Duhr and D. Braun, Why molecules move along a temperature gradient, *Proc. Natl. Acad. Sci. U. S. A.*, 2006, **103**, 19678–19682.
57 D. Chatterjee, A. Singla, D. Chatterjee, B. S. Vishnugopi and P. P. Mukherjee, Thermal Modulation of Electrodeposition Stability in Sodium Metal Electrodes, *Adv. Sci.*, 2026, **13**, e15275.
58 A. F. Chadwick, *et al.*, Suppression of Dendrites in Metal-Anode Batteries by the Soret and Seebeck Effects, *ACS Energy Lett.*, 2025, **10**, 6281–6287.
59 D. Chatterjee, K. G. Naik, B. S. Vishnugopi and P. P. Mukherjee, Electrodeposition Stability Landscape for Solid-Solid Interfaces, *Adv. Sci.*, 2024, **11**, e2307455.
60 M. Ganser, *et al.*, An Extended Formulation of Butler-Volmer Electrochemical Reaction Kinetics Including the Influence of Mechanics, *J. Electrochem. Soc.*, 2019, **166**, H167–H176.
61 A. Mistry and P. P. Mukherjee, Molar Volume Mismatch: A Malefactor for Irregular Metallic Electrodeposition with Solid Electrolytes, *J. Electrochem. Soc.*, 2020, **167**, 082510.
62 M. J. Wang, J. Y. Chang, J. B. Wolfenstine and J. Sakamoto, Analysis of elastic, plastic, and creep properties of sodium metal and implications for solid-state batteries, *Materialia*, 2020, **12**.
63 C. D. Fincher, Y. Zhang, G. M. Pharr and M. Pharr, Elastic and Plastic Characteristics of Sodium Metal, *ACS Appl. Energy Mater.*, 2020, **3**, 1759–1767.
64 X. Zhang, Q. J. Wang, B. Peng and Y. Wu, Pressure-Driven and Creep-Enabled Interface Evolution in Sodium Metal Batteries, *ACS Appl. Mater. Interfaces*, 2021, **13**, 26533–26541.
65 G. S. Zhang, *et al.*, In Situ Measurement of Radial Temperature Distributions in Cylindrical Li-Ion Cells, *J. Electrochem. Soc.*, 2014, **161**, A1499–A1507.
66 Y. Troxler, *et al.*, The effect of thermal gradients on the performance of lithium-ion batteries, *J. Power Sources*, 2014, **247**, 1018–1025.